A New High-Gain Microstrip Yagi Array Antenna With a High Front-to-Back (F/B) Ratio for WLAN and Millimeter-Wave Applications

Gerald R. DeJean, *Student Member, IEEE*, and Manos M. Tentzeris, *Senior Member, IEEE*

***Abstract*—A new printed microstrip Yagi array antenna is proposed that can achieve a high gain and low backside radiation for various applications up to the millimeter-wave frequency range. The high front-to-back (F/B) ratio (up to 15 dB) is attributed to the constructive interference that takes place between the individual printed Yagi arrays in the design. Through the spacing of the elements, the directivity (between 9–11.5 dBi) and the F/B ratio can be altered to suit the application of interest. The operational principles of this design are discussed to give insight on the radiation mechanism of the antenna. An initial design at around 32.5 GHz is presented to show the performance capabilities of this configuration. An impedance bandwidth of 8.3% can be achieved around this frequency. Then, a parametric analysis is conducted to estimate the significance of the design parameters that affect the antenna's performance. Finally, measured return loss and radiation pattern performance at 5.2 GHz is displayed to validate the principles and simulated results of the design. The measured impedance bandwidth of 10% is achieved. The F/B ratio is 15 dB which is larger than values previously published by 5–10 dB. Additionally, a gain of 10.7 dBi is observed. To the author's knowledge, this is the first microstrip Yagi array antenna presented that has a high gain and a high F/B ratio designed using simple fabrication techniques.**

***Index Terms*—Front-to-back (F/B) ratio, gain, microstrip Yagi array, quasi endfire.**

I. Introduction

THE explosive growth of the wireless communications industry has led to an increasing demand for low cost, low profile antennas that can be printed on a substrate. Printed antennas enjoy many advantages over standard antennas, such as low manufacturing costs, low profile, ease of integration with monolithic microwave integrated circuits (MMICs) and integrated passives, and the ability to be mounted on planar, nonplanar, and rigid exteriors [1]. Although most wireless local area network (WLAN) applications utilize omnidirectional antennas, directional and quasi endfire antennas, such as Yagi arrays, have been employed to suppress unwanted radio frequency (RF) emissions as well as unwanted interference in other directions. Yagi arrays have been utilized in industrial, scientific, and medical (ISM) applications at 2.4 GHz (where directional radiation is necessary for long distance wireless communications and point-to-point communications), high performance radio local area network (HIPERLAN) and IEEE802.11a (IEEE802.11n) WLAN bands between 5–6 GHz (where quasi endfire radiation in the range between 0°–90° enables efficient communications at rates between 20–54 megabits per second), and ultra-broadband, millimeter-wave applications (above 30 GHz) that require high gain (>10 dBi), quasi endfire radiation to alleviate propagation loss effects through line-of-sight reception of waves at angles off broadside for wireless video transfer, millimeter-wave ad-hoc sensor networks, and point-to-multipoint wideband links. The Yagi arrays currently on the market [2], [3] that operate at the lower frequencies (under 10 GHz) are too bulky and are unsuitable for compact integration with microwave monolithic integrated circuits (MMICs) and RF circuitry due to their size.

There have been many printed Yagi antenna configurations that have been presented over the last 15 years [4]–[10]. The use of Yagi antenna designs in microstrip technology was first proposed by Huang in 1989 which consists of four patches (one reflector, one driven element, and two directors) that electromagnetically coupled to one another to create a steering of the main beam to a peak between 30°–40° [4]. To increase the gain, Densmore and Huang introduced microstrip Yagi arrays (each consisting of four elements) in four rows and excited the driven elements simultaneously [5], [6]. This design can achieve a peak gain as high as 14 dBi, but F/B ratios around 4–5 dB may not be suitable for some applications. In [7], a successful attempt to improve the gain of a single microstrip Yagi array using a periodic bandgap (PBG) structure was proposed. This approach takes away from the manufacturing simplicity of using a double-clad board. In general, there is a tradeoff between achieving a high gain and maintaining a high F/B ratio and low cross-polarization for existing printed Yagi antenna arrays. Additionally, there has been one Yagi array that has been proposed for millimeter wave frequencies that radiates in the endfire direction with a high gain [8].

In this paper, a new microstrip Yagi array design is presented that can achieve a high gain (>10 dBi) without compromising the low cross-polarization and high F/B ratio; qualities that are essential for the design of a planar antenna geometry that can be easily integrated with wireless communicational devices. Note in this paper, the F/B ratio is the ratio of frontside radiation in the range of $0^\circ \leq \theta \leq 90^\circ$ to backside radiation in the range of $-90^\circ \leq \theta \leq 0^\circ$. A numerical investigation is presented to explain the coupling mechanism of the design. Moreover, a para-

Manuscript received February 19, 2006; revised July 25, 2006.

The authors are with the Georgia Electronic Design Center, School of Electrical and Computer Engineering, Georgia Institute of Technology, Atlanta, GA 30332-0250 USA (e-mail: gdejean@ece.gatech.edu).

Color versions of one or more of the figures in this paper are available online at http://ieeexplore.ieee.org.

Digital Object Identifier 10.1109/TAP.2006.889818

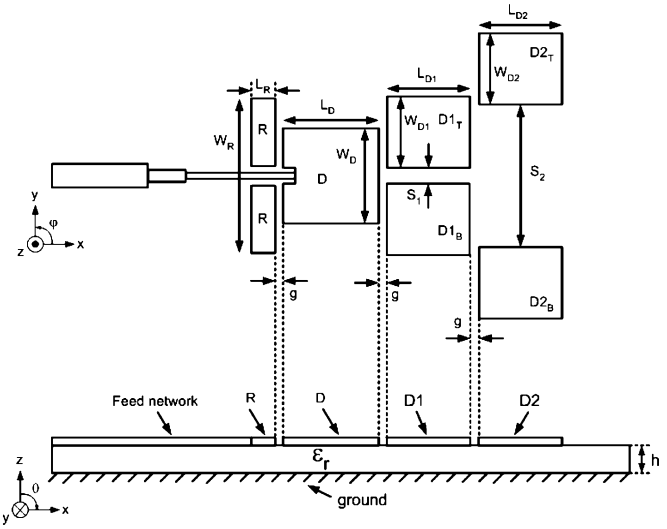

Fig. 1. Yagi antenna structure.

metric study is conducted to understand the critical parameters that affect the performance of the design. The design techniques proposed in this analysis are applied to millimeter wave applications above 30 GHz, but this configuration is easily scalable to lower frequency applications such as the ISM band at 2.4 GHz and HIPERLAN applications at 5.2 GHz.

II. Antenna Structure

The antenna architecture is shown in Fig. 1. It consists of seven patch elements as well as the feeding structure. The reflector elements R, will be treated as one single element with a gap through the middle to simplify the analysis. The driven element D, is excited by a simple feeding structure through a gap in the reflector elements. The feeding structure consists of a 50 Ω feedline that is transformed to a high impedance line through the use of a quarter-wave transformer. High impedance line (width less than 0.15 times a patch length) are utilized to ensure that the feedline radiation close to the driven element will not disrupt the radiation of the antenna and lead to an increased F/B ratio. The remaining elements include four directors: $\mathrm{D1_T}$ (top director1), $\mathrm{D1_B}$ (bottom director1), $\mathrm{D2_T}$ (top director2), and $\mathrm{D2_B}$ (bottom director2). This antenna structure is designed on a double copper (Cu) clad board of RT/duroid 5880 material ($\varepsilon_r = 2.2$). The lengths and widths of the patch elements are denoted as follows: for the reflector R, the length and width are $\mathrm{L_R}$ and W_R; for the driven element D the length and width are $\mathrm{L_D}$ and W_D; for the director1 elements $\mathrm{D1_T}$ and $\mathrm{D1_B}$, $\mathrm{L_{D1}}$ and W_{D1} represent the length and width; and the length and width of the director2 elements $\mathrm{D2_T}$ and $\mathrm{D2_B}$ are $\mathrm{L_{D2}}$ and W_{D2}. The distance between the elements along the x-axis is denoted by g (note that these distances are the same). Furthermore, the distances between the director1 and director2 elements are represented by $\mathrm{S_1}$ and $\mathrm{S_2}$, respectively. The thickness of the substrate, shown in Fig. 1, is denoted by h.

III. Principles of Operation

The mechanism of gain enhancement can be seen through the constructive interference between the $\mathrm{R-D-D1_T-D2_T}$ and the $\mathrm{R-D-D1_B-D2_B}$ single microstrip Yagi arrays. This constructive interference can be viewed as one that is analogous to the radiation mechanism of a patch antenna and its radiating slots. For the design proposed in Fig. 1, the single $\mathrm{R-D-D1_T-D2_T}$ array has a peak radiation at $10^\circ \leq \varphi \leq 16^\circ$, while the $\mathrm{R-D-D1_B-D2_B}$ array radiates maximally at $-16^\circ \leq \varphi \leq -10^\circ$. The total microstrip Yagi array (Fig. 1) has a maximum radiation at $\varphi = 0^\circ$ with a higher gain. Consequently, the increased gain of the new antenna structure considerably decreases the backside radiation. This is due to the constructive interference between the single microstrip Yagi arrays that pulls more power away from the reflector side of the driven element and towards the $\varphi = 0^\circ$ quasi-endfire direction. This decrease allows the effect of the reflector patch to be minimal. Through simulation, the length, $\mathrm{L_R}$, of the reflector is designed to be about 1/4 is total width, W_R. A shorter length can result in increased backside radiation. A larger length is unnecessary for reducing the backside radiation (it will only increase the size of the design, while the radiation performance will stay the same). Feeding through the reflector has negligible effect on the impedance mismatch between the microstrip-coplanar waveguide (CPW) transition because the impedance difference between the lines is less than 5 Ω and both lines have impedances above 100 Ω.

The design of the microstrip Yagi array proposed in this paper consists of two major effects that are taking place to result in a higher gain and higher F/B ratio: the role of D1 elements ($\mathrm{D1_T}$ and $\mathrm{D1_B}$) and the spacing between them ($\mathrm{S_1}$) and the role of D2 elements ($\mathrm{D2_T}$ and $\mathrm{D2_B}$) and the spacing between them ($\mathrm{S_2}$). The D1 elements are used to establish the directionality of the beam as well as increase the impedance bandwidth of the antenna due to the close proximity between the resonant modes of D1 and the driven element. (Note that since the resonant length of D1 is slightly shorter than the driven element, it will resonate at a slightly higher frequency, but the combination of these modes will produce an increase in bandwidth.) On the other hand, the D2 patches are used to increase the gain of the design. Both concepts are explained further.

The $\mathrm{S_1}$ parameter has to be small in order to strongly couple fields from the driven element to the D1 elements. When a parasitic element is placed next to a driven element, its distance has to be small ($< 0.05\lambda_{\mathrm{eff}}$ where $\lambda_{\mathrm{eff}} = c/(f_r^* \varepsilon_{\mathrm{eff}}\text{^}0.5)$ and $\varepsilon_{\mathrm{eff}}$, the effective dielectric constant, lies in the range of $1 < \varepsilon_{\mathrm{eff}} < \varepsilon_r$) in order to increase the gap capacitance between the driven and D1 elements. An equivalent circuit that models the gap between the driven element and one D1 element is illustrated in Fig. 2 where C_F and C_G are the fringe field and gap capacitances, respectively. Equations for solving for C_F and C_G are presented in [11]. As the D1 elements are separated further apart from each other, the gap capacitance decreases because the parallel plate area A ($A = t_C * W_P$ where t_C is the thickness of the conductor and W_P is the parallel plate width), between the elements is smaller (W_P decreases). This decrease in the gap capacitance results in a decrease of electric field coupling to the resonant D1 elements. The surface current distributions in Fig. 3 display this effect.

The D2 elements serve the sole of purpose of enhancing the gain of the antenna. It is observed through simulation that the

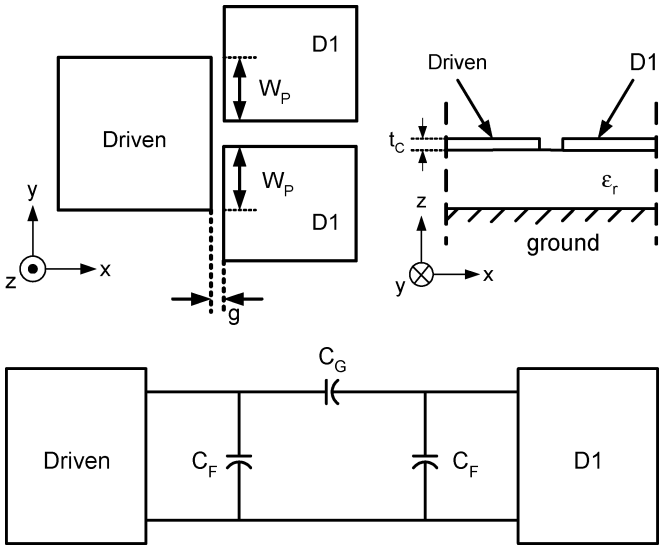

Fig. 2. Schematic of driven element and D1 element and its equivalent circuit.

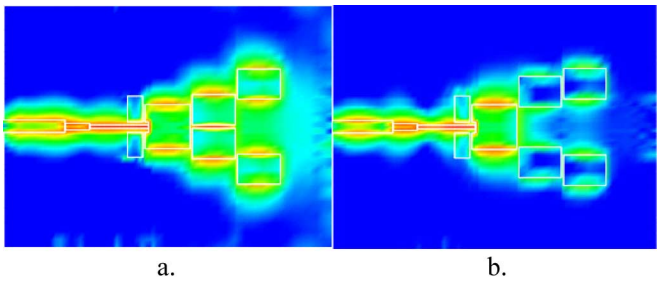

Fig. 3. Surface current distributions on the conductors for (a) $S_1 = 0.04\lambda_{\text{eff}}$ and (b) $S_1 = 0.40\lambda_{\text{eff}}$.

small value of S_1 (close placement of the D1 elements with respect to each other) has a major effect on the radiating edges of the D1 elements. In particular, the radiating edges of the D1 elements act as a single radiating edge with width $2W$. Considering the strong magnitude of the electric fields at the edge as well as the strong fringing fields of the closely spaced D1 elements, the placement of the D2 elements is arbitrary with respect to receiving enough fringe field coupling to necessitate radiation. In other words, the D2 elements can be placed at many positions along the y-direction and still receive coupling (S_2 can range in value). Although, there are many possibilities for S_2 for receiving coupling, this parameter does have a significant effect on the gain of the antenna. As S_2 increases, the separation between the D2 elements also increases and the gain is improved because the effective aperture is electrically wider. The surface current distributions (Fig. 4) show this effect. There is a limit on the value of S_2. If S_2 becomes too large ($> 0.55\lambda_{\text{eff}}$), there will be insufficient coupling between the D1 and D2 elements and the enhancement of the gain will be suppressed.

Similar to what has been stated in previous microstrip Yagi papers [7], the addition of a 3rd set of director elements (D3) does not improve the gain of the Yagi array. This is due to the fact that the fields in the aperture become weaker as they propagate away from the D1 elements.

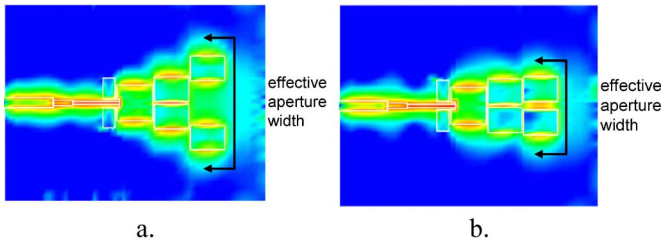

Fig. 4. Surface current distributions on the conductors for (a) $S_2 = 0.55\lambda_{\text{eff}}$ and (b) $S_2 = 0.10\lambda_{\text{eff}}$.

IV. Initial Design

A design has been simulated using MicroStripes 6.5 as a proof of concept to cover a band above and below 32.5 GHz suitable for millimeter wave applications. MicroStripes 6.5 is a 3-D full-wave simulator that solves for the electric and magnetic fields via the transmission line matrix (TLM) method. Fig. 5 shows a plot of the return loss versus frequency for this design. The values of the design parameters are as follows: $L_R = 1000\ \mu$m, $W_R = 4016\ \mu$m, $L_D = W_D = 2956\ \mu$m, $L_{D1} = L_{D2} = 2814\ \mu$m, $W_{D1} = W_{D2} = 2014\ \mu$m, $S_1 = 286\ \mu$m, $S_2 = 3686\ \mu$m, and $g = 140\ \mu$m. The substrate thickness is 254 μm. These values represent the optimized values for this design in terms of highest achievable directivity and F/B ratio greater than or equal to 15 dB. There are two resonances that are present in the plot. The lower frequency resonance is the TM_{10} resonance of the driven element D, while the higher frequency resonance is associated with the director1 D1, elements that have a slightly shorter length. The optimized bandwidth is 8.3% due to the close proximity of the two resonances. The E-plane radiation patterns are shown at three frequencies (31.7, 32.3, 32.7, and 33.1 GHz) in Fig. 6(a). In addition, Fig. 6(b) shows the E-plane patterns at the -10 dB low and high edge frequencies (f_L and f_H). The scales are normalized with respect to the maximum E-plane radiation of the antenna. It is observed that as the frequency increases, the F/B ratio decreases. At 32.3 GHz, there is no significant backlobe present and the beamwidth is slightly wider. This can be attributed to the fields that are more concentrated around the driven element which resonates around that frequency. The directivity is 11.1 dBi, and the scan angle is 31.5°. At 32.7 GHz, the F/B ratio is 15 dB and a scan angle of 35.5° with an E-plane beamwidth (-3 dB) of 40° is observed at this frequency. This F/B ratio is much higher than some values previously published that are between 5–10 dB [5]–[9]. A directivity of 11.4 dBi is achieved at this frequency. At 33.1 GHz, there exist two backside lobes that are -15 dB and -8 dB down from the main beam. In this case, the radiation from the D1 elements is stronger than radiation from the driven element. Although there is a significant contribution of radiation from the driven element, the fields of the driven and D1 elements are out of phase. The directivity at this frequency is 11.1 dBi, and the scan angle has increased to 42°. At f_L, the pattern exhibits strong broadside characteristics, while at f_H, the grating lobes are significant in comparison to the main beam.

Although the impedance bandwidth is 8.3%, the useful radiation bandwidth is smaller, but this is dependent on the application and the desired specifications of F/B ratio and direc-

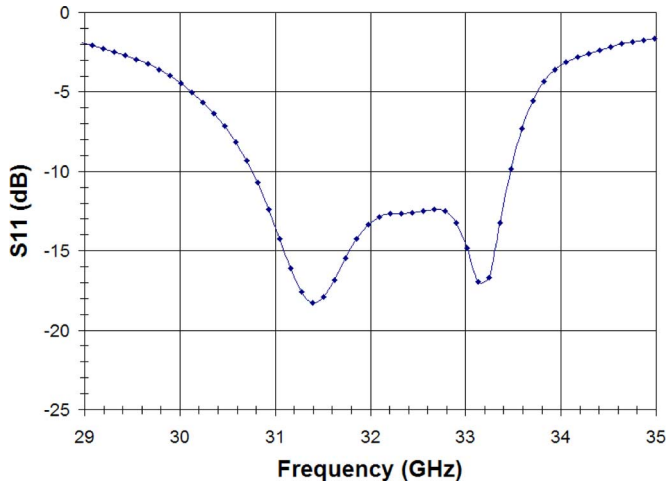

Fig. 5. Return loss versus frequency of Yagi structure in Fig. 1 covering band above and below 32.7 GHz.

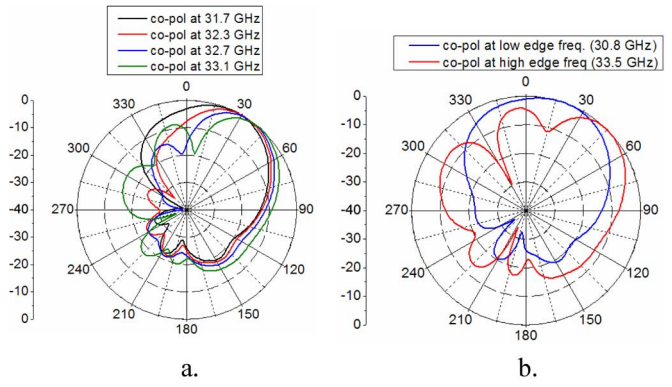

Fig. 6. E-plane co-polarized components of Yagi structure in Fig. 1 at (a) 31.7, 32.3, 32.7, and 33.1 GHz and at (b) 30.8 and 33.5 GHz.

tivity. If a designer wants a 14 dB F/B ratio with a directivity greater than 10 dBi and a maximum radiation angle greater than 20°, then the radiation bandwidth may be less than 1%. However, (as stated in the following example) if a designer wants only a 10 dB F/B ratio then the radiation bandwidth may be as much as 7%. The radiation pattern starts to exhibit the quasi endfire radiation characteristic (seen in microstrip Yagi arrays) at about 31.5 GHz. At frequencies below 31.5 GHz, the antenna radiates a broadside wave due to the current distribution that exists mainly on the driven element. Between 31.5–32.7 GHz $(\text{bandwidth} = 3.7\%)$, a F/B ratio greater than 15 dB can be achieved. A greater than 40° −3dB-beamwidth is observed between 31.5–33.2 GHz $(\text{bandwidth} = 5.2\%)$. In addition, limits on the gain and the angles of maximum radiation will help determine what the radiation bandwidth will be for a specific application. The impedance bandwidth and radiation bandwidth will be approximately equal when the acceptable F/B ratio is greater than 4 dB.

The azimuth radiation patterns (on the plane parallel to the antenna) at the angle θ, of maximum radiation are shown in Fig. 7 at 31.7, 32.3, 32.7, and 33.1 GHz. The E_θ components of the azimuth plane radiation pattern at the three frequencies illustrate a reduction of greater than 16 dB at $\varphi = 180°$ with respect to the direction of maximum radiation along the positive x-axis

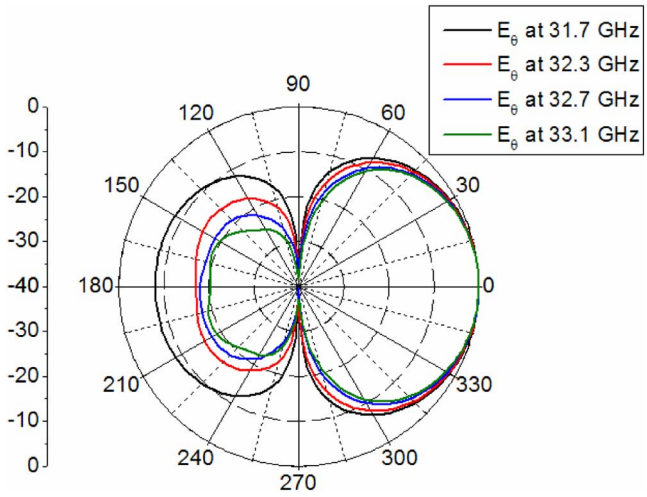

Fig. 7. E_θ components at 31.7, 32.3, 32.7, and 33.1 GHz.

$(\varphi = 0°)$ for frequencies greater than 32.3 GHz. The −3 dB azimuthal beamwidths are between 72–75°. Finally, low levels of cross-polarization are obtained at all frequencies considered in this design.

V. Parametric Analysis

There are many parameters that need to be addressed in this antenna structure due to the number of elements, coupling gaps, and distances between patches. This section gives insight on how these critical parameters affect the radiation characteristics presented in the tables of this section. These parameters are varied around the optimized values given in the previous section. The simulated cross-polarization is better than 30 dB below the main beam and the −3 dB beamwidths are between 40–42° in all of the parameters analyzed, so no mention of these characteristics will be discussed in this section.

A. Variation of Width S_2 at 32.7 GHz

The dimension, S_2, is the first parameter that was varied, and the effects of this variation are summarized in Table I. For this variation, all variables are initially set to the optimized values given in Section IV. From this table, it can be observed that this parameter has a major affect on the directivity and F/B ratio because this parameter increases or decreases the effective aperture width of the antenna. When this value is larger, the directivity and F/B ratio is greatly increased. Smaller values have a severe effect on the F/B ratio. As the value of L_2 is increased, the antenna size in the y-direction is increased. A width of 3686 μm $(\sim 0.55\lambda_{\text{eff}})$ represents the largest possible value in which enough energy is coupled from the D1 elements. If S_2 becomes larger, energy from D1 will not couple to D2 (as explained earlier). This value also represents the highest directivity and F/B ratio that can be obtained for this design.

B. Variation of Width S_1 at 32.7 GHz

The variation of width S_1 is summarized in Table II. Again, all variables are initially set to the optimized values discussed in the last section. From the table, it is seen that the directivity and the F/B ratio is critically affected by the change in S_1. As S_1 increases, the directivity is decreased by as much as 2.4 dBi, while

TABLE I

S_2 (μm)	Directivity (dBi)	E-plane angle of max rad.(deg)	F/B Ratio (dB)
3686	11.4	35.5	15
3086	11.3	38	10
2486	11.3	36.6	8
1886	11.1	36.6	8
1286	10.8	37	6
686	10.6	36.7	5

TABLE II

S_1 (μm)	Directivity (dBi)	E-plane angle of max rad.(deg)	F/B Ratio (dB)
286	11.4	35.5	15
886	11.3	35.3	11
1486	11.0	36.2	7
2086	10.2	37.4	5
2686	9.0	37.5	2

the F/B ratio is reduced by as much as 13 dB. The major reason for this decline in directivity and F/B ratio is the decreased coupling from the driven element to the D1 element as a result of the decreased gap capacitance. The scan angle has minimal effect in this study. The optimal electrical value of 0.043 λ_{eff} (286 μm) seems to be the suitable width, S_1, for this application because it gives the highest directivity and F/B ratio. This parameter may possibly have a smaller value at lower frequencies where the wavelength is much larger.

C. Variation of the Gap g at 32.7 GHz

The gap g is a very important parameter to analyze because it affects the coupling of the patch elements. Values of various gaps are summarized in Table III. As this value increases, the directivity, scan angle, and F/B ratio is affected. The directivity decreases by as much as 2.3 dBi, while the F/B ratio severely diminishes by as much as 13 dB as the gap size is increased from 140 μm to 300 μm. The decrease in F/B ratio is due to the fact that the major contribution of radiation comes from the driven element and edge diffraction effects from a large size finite substrate that causes the main beam to split into two lobes with a small F/B ratio (2–3 dB). Additionally, as g is increased, the scan angle tends to increase as well since the broadside radiation of the driven element becomes more intense and a second lobe is present in the radiation at broadside. The formation of this lobe gradually pushes the maximum radiation of the quasi endfire main lobe to a higher angle. When g becomes too large ($> 0.028\lambda_{\text{eff}}$), the presence of the D1 elements have no effect on the driven element, and therefore, you only have the driven element that is radiating. The difference between 0.021 λ_{eff} (140 μm) and 0.045 λ_{eff} (300 μm) in selecting the gap width can be quite crucial. As shown in Table III, a 50 μm difference in the gap size (140–190 μm) results in a 5 dB difference in the F/B ratio and a difference in the gain of the antenna. To get a better idea of the F/B ratio and gain of the antenna at smaller intervals of change in the gap size as well as identifying the sensitivity of this parameter on the design, simulations were conducted starting at a gap size of 140 μm with a $+5$ μm increment up to 200 μm. In our analysis, it was shown that at 140 μm, a directivity of 11.4 dBi and F/B ratio of 15 dB is given. At 200 μm, a directivity of 11.0 dBi and F/B ratio of around 9 dB is observed. At all gap sizes in between 140 and 200 μm, the directivity and F/B ratio decreases monotonically from $g = 140$ μm $g = 200$ μ. Overetching can diminish the desired gain and desired F/B ratio. It is also worth noting that a 60 μm increase in the gap from the desired value of 140 μm still results in a 10 dB F/B ratio which is improved in comparison with past research of these antenna types.

TABLE III

g (μm)	Directivity (dBi)	E-plane angle of max rad.(deg)	F/B Ratio (dB)
140	11.4	35.5	15
190	11.1	37.2	10
240	10.5	39.9	6
300	9.2	44.2	2

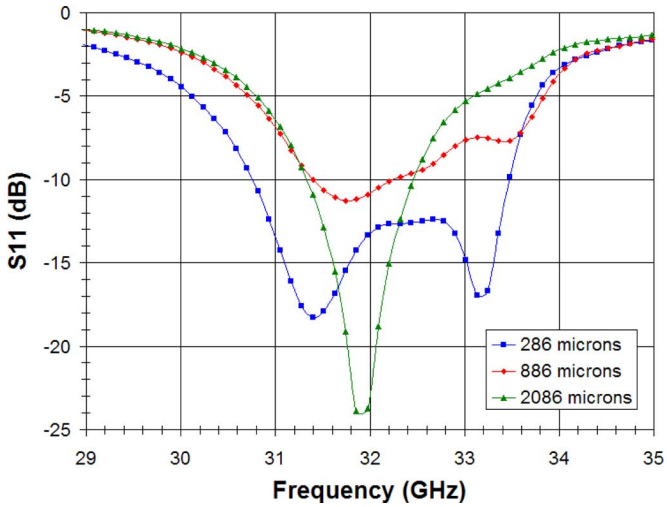

Fig. 8. Return loss versus frequency at three values of S_1.

D. Effects on Bandwidth Variation

The bandwidth of the design is mostly controlled by the S_1 parameter which is the spacing of the D1 elements. This is because the D1 elements are also resonant (as well as the driven element). When the coupling between the elements (driven and D1s) is strong, the D1 elements are excited electromagnetically. Since the resonant lengths of the driven and D1 elements are close in value, two TM_{10} resonance peaks are present, which are also close in frequency, and the bandwidth of the antenna is significantly larger (close to 8%). On the other hand, as the value of S1 becomes larger, the coupling is reduced to a point where there is no coupling between the driven and D1 elements. Therefore, the driven element is the only resonant element present and hence, the bandwidth is suppressed (about 4%) due to the elimination of the TM_{10} mode of the D1 element. This is seen in Fig. 8 at three values of S_1. As S_1 increases, the higher resonance gradually decreases to a point when only the driven patch resonance is present. The effect of S_1 serves to steer the main beam as well as broaden the bandwidth of the design.

VI. Simulated and Measured Results

To verify the analysis that has been presented for this antenna structure, a scaled design was simulated around a band

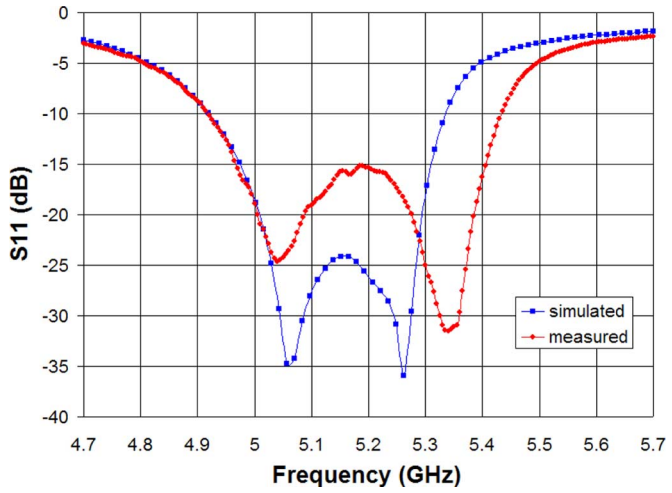

Fig. 9. Return loss versus frequency for prototype at a band around 5.2 GHz. Physical dimensions are as follows: $L_R = 245$ mils, $W_R = 1002$ mils, $L_D = W_D = 724$ mils, $L_{D1} = L_{D2} = 688$ mils, $W_{D1} = W_{D2} = 492$ mils, $S_1 = 72$ mils, $S_2 = 902$ mils, $g = 35$ mils. Substrate: RT/Duroid 5880 ($\varepsilon_r = 2.2$, $\tan\delta = 0.0009$ @ 10 GHz) with thickness = 62 mils.

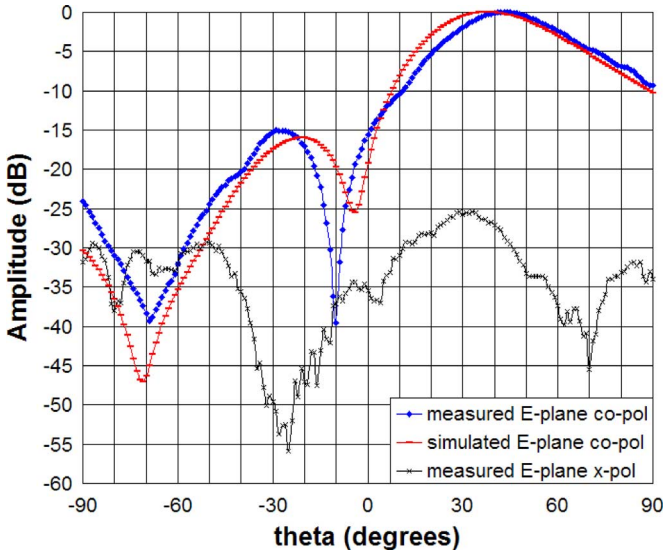

Fig. 10. E-plane radiation patterns in rectangular form at 5.2 GHz.

above and below 5.2 GHz for HIPERLAN applications. This design was fabricated by Prototron Circuits, Inc., and measured in the high frequency laboratory of Technology Square Research Building (TSRB) at Georgia Tech.

For the return loss measurement, an edge-mount SMA connector was soldered to the edge of the board, and the return loss was measured on a network analyzer. The simulated and measured return loss versus frequency is presented in Fig. 9. (The physical dimensions of this design are shown in the caption of Fig. 9.) There are two frequency shifts in the resonances of the measured design when compared to the simulated results. The lower resonance has a frequency shift of 20 MHz which is small for this design, but the frequency shift of 80 MHz at the higher resonance can possibly be attributed to a small tolerance in the substrate (RT/Duroid 5880, $\varepsilon_r = 2.2 \pm 0.02$) and/or overetching of the metal. Additionally, the return loss at the resonances is higher (more reflection), but definitely acceptable for this application. The connector was not taken into account in the simulation. The bandwidth of the measured prototype (10%) is considerably larger than the simulated design (7.8%). This can be mainly attributed to the shift in frequency at the higher resonance. The broadened bandwidth of the measured design may not be suitable for narrowband applications. The size of the ground plane is $1.95\lambda_0 \times 1.95\lambda_0$. To analyze the effect of the ground plane on the structure, the ground plane was increased 12 times up to a factor of 120% in increments of 10% of the current size in both directions ($-x$ and $-y$). This study showed that as the ground plane increases from 10% to a factor of 40% of the current size, the directivity decreases by small increments (about 0.3 dBi) and the front to back decreases from around 15 to 11–12 dBi. Ground size enlargements from 50% to 120% result in the main beam becoming degraded to a point where the beam split into two. This is largely due the edge diffraction effects that occur at the edges of the substrate when the ground plane is large.

The radiation pattern was measured in the anechoic chamber of TSRB. The antenna was mounted on a metallic platform by using tape and connected to a coaxial cable. The antenna-under-test (AUT) served as the transmitting antenna, while, a WR159 (4.9–7.05 GHz) rectangular horn antenna was used to receive the wave. The E-plane radiation pattern was measured at 5.225 GHz and compared to the simulated results. This is shown in Fig. 10. Due to the design of the chamber, only an E-plane measurement in the range of $-90° \leq \theta \leq 90°$ could be taken. This is sufficient to compare the main beam and the backside radiation level ($-90° \leq \theta \leq 0°$). The co-polarized components of the measured and simulated designs are in good agreement with each other. The main beam has been shifted by 8°. This may be attributed to the stronger concentration of fields on the D1 elements as opposed to the driven element. The measured F/B ratio is 15 dB which is a significant improvement over other designs presented in past literature. The measured -3 dB beamwidth is 38° ($26° \leq \theta \leq 64°$). This is due to the sharp decline in amplitude between 12–18°. The gain of the antenna is 10.7 dBi with an efficiency greater than 85%. The cross-polarized component of the measured design is 25 dB below the main beam.

VII. Conclusion

A microstrip Yagi array antenna design has been presented for various frequency bands to be integrated to ISM, IEEE802.11a (IEEE802.11n), and millimeter wave applications. Bandwidths greater than 7.5% can be achieved through the use of the two close resonances of the driven and director elements. Quasi endfire radiation in the range of 40° can be achieved by the configuration of this design. A high F/B ratio (15 dB) and a low cross polarization is achieved which is suitable for applications where the backside level needs to be suppressed. Finally, a high gain (>10 dB) is observed through the use of multiple directors (four total: two D1 and two D2 elements) and the idea of constructive interference. To the author's knowledge, this is the first microstrip Yagi array design that has been proposed that can simultaneously achieve high gain quasi endfire radiation with a high F/B ratio.

REFERENCES

[1] D. Pozar, "Microstrip antennas," *Proc. IEEE*, vol. 80, no. 1, pp. 79–91, Jan. 1992.

[2] [Online]. Available: http://www.manufacturers.com.tw/telecom/Yagi-Antenna.html

[3] [Online]. Available: http://www.starantenna.com

[4] J. Huang, "Planar microstrip Yagi array antenna," in *IEEE Antennas and Propagation Society Int. Symp.*, Jun. 1989, vol. 2, pp. 894–897.

[5] A. Densmore and J. Huang, "Microstrip Yagi antenna for mobile satellite service," in *IEEE Antennas and Propagation Society Int. Symp.*, Jun. 1991, vol. 2, pp. 616–619.

[6] J. Huang and A. Densmore, "Microstrip Yagi antenna for mobile satellite vehicle application," *IEEE Trans. Antennas Propag.*, vol. 39, no. 7, pp. 1024–1030, Jul. 1991.

[7] S. Padhi and M. Bialkowski, "Investigations of an aperture coupled microstrip Yagi antenna using PBG structure," in *IEEE Antennas and Propagation Society Int. Symp.*, Jun. 2002, vol. 3, pp. 752–755.

[8] P. R. Grajek, B. Schoenlinner, and G. M. Rebeiz, "A 24 GHz high-gain Yagi-Uda antenna array," *IEEE Trans. Antennas Propag.*, vol. 52, no. 5, pp. 1257–1261, May 2004.

[9] D. Gray, J. Lu, and D. Thiel, "Electronically steerable Yagi-Uda microstrip patch antenna array," *IEEE Trans. Antennas Propag.*, vol. 46, no. 5, pp. 605–608, May 1998.

[10] S. Ke and K. Wong, "Rigorous analysis of rectangular microstrip antennas with parasitic patches," in *IEEE Antennas Propag. Society Int. Symp.*, Jun. 1995, vol. 2, pp. 968–971.

[11] K. Gupta, R. Garg, I. Bahl, and P. Bhartia, *Microstrip Lines and Slotlines*. Boston, MA: Artech House, 1996.

Gerald R. DeJean (S'03) received the B.Sc. degree in electrical engineering (*summa cum laude*) from Michigan State University, East Lansing and the M.S. degree in electrical and computer engineering from the Georgia Institute of Technology (Georgia Tech), Atlanta, in 2000 and May 2005, respectively. He is currently working towards the Ph.D. degree in electrical and computer engineering at Georgia Tech, to be completed in May 2007.

He has worked on a number of research projects as a member of the NSF Packaging Research Center and the Georgia Electronic Design Center. He has authored and coauthored over 30 papers in refereed journals and conference proceedings. His research interests include antenna design, RF/microwave design and characterization, and 3-D system-on-package (SOP) integration of embedded functions that focuses largely on modern commercial RF systems such as cellular phones for PCS applications, Bluetooth and 2.4 GHz ISM applications, RFID's, WLAN (802.11a,b,g), LMDS, and millimeter-wave applications at 60 GHz. He has dedicated his graduate research to making the antenna more compact and integrable with multilayer packages such as low temperature cofired ceramic (LTCC), liquid crystal polymer (LCP), and multilayer organic (MLO) while maintaining the full functionality of the device for wideband and/or multiband applications. He is also interested in equivalent circuit modeling techniques to assist in the design and optimization of compact antennas.

Mr. DeJean is a member of the Eta Kappa Nu and Tau Beta Pi national honor societies. He was awarded the prestigious Microsoft Research Fellowship Award for Excellence in Graduate Research and was twice a finalist in the student paper competition of the 2004 and 2005 IEEE Antennas and Propagation Society Symposia.

Manos M. Tentzeris (S'89–M'98–SM'03) received the diploma degree in electrical and computer engineering (*magna cum laude*) from the National Technical University of Athens, Greece, and the M.S. and Ph.D. degrees in electrical engineering and computer science from the University of Michigan, Ann Arbor.

He was a Visiting Professor with the Technical University of Munich, Germany for the summer 2002, where he introduced a course in the area of high-frequency packaging. He has given more than 50 invited talks in the same area to various universities and companies in Europe, Asia and America. He is currently an Associate Professor with the School of Electrical and Computer Engineering, Georgia Institute of Technology (Georgia Tech), Atlanta. He has helped develop academic programs in highly integrated/multilayer packaging for RF and wireless applications, microwave MEMs, SOP-integrated antennas and adaptive numerical electromagnetics (FDTD, multiresolution algorithms) and heads the ATHENA Research Group (15 researchers). He is the Georgia Electronic Design Center Associate Director for RFID/sensors research, the Georgia Tech NSF-Packaging Research Center Associate Director for RF Research and the RF Alliance Leader. He is also the leader of the RFID Research Group of the Georgia Electronic Design Center (GEDC) of the State of Georgia. He has published more than 250 papers in refereed journals and conference proceedings, one book and eight book chapters and is in the process of writing two books.

Dr. Tentzeris is a member of the International Scientific Radio Union (URSI) Commission D, an Associate Member of EuMA, and a member of the Technical Chamber of Greece. He was the recipient of the 1997 Best Paper Award of the International Hybrid Microelectronics and Packaging Society for the development of design rules for low-crosstalk finite-ground embedded transmission lines. He received the 2000 NSF CAREER Award for his work on the development of MRTD technique that allows for the system-level simulation of RF integrated modules, the 2001 ACES Conference Best Paper Award, the 2002 International Conference on Microwave and Millimeter-Wave Technology Best Paper Award (Beijing, China) for his work on compact/SOP-integrated RF components for low-cost high-performance wireless front-ends, the 2002 Georgia Tech-ECE Outstanding Junior Faculty Award, the 2003 NASA Godfrey "Art" Anzic Collaborative Distinguished Publication Award for his activities in the area of finite-ground low-loss low-crosstalk coplanar waveguides, the 2003 IBC International Educator of the Year Award, the 2003 IEEE CPMT Outstanding Young Engineer Award for his work on 3-D multilayer integrated RF modules, and the 2004 IEEE TRANSACTIONS ON ADVANCED PACKAGING Commendable Paper Award. He was also the recipient of the 2006 IEEE MTT Outstanding Young Engineer Award. He was the 1999 Technical Program Co-Chair of the 54th ARFTG Conference, Atlanta, GA and he is the Vice-Chair of the RF Technical Committee (TC16) of the IEEE CPMT Society. He has organized various sessions and workshops on RF/Wireless Packaging and Integration in IEEE ECTC, IMS, and APS Symposia in all of which he is a member of the Technical Program Committee in the area of "Components and RF." He is an Associate Editor of the IEEE TRANSACTIONS ON ADVANCED PACKAGING.